

Invited Paper

# ToF-SIMS Imaging of Intracellular $^{39}\text{K}/^{40}\text{Ca}$ Changes induced by ZnO-containing Nanomaterials

Pei-Ling Lee,<sup>1,2</sup> Sin-Yu Shen,<sup>3</sup> Yu-Sheng Yin,<sup>1</sup> Shiu-Ling Lei,<sup>1</sup> Cian-Ling Jhang,<sup>4</sup> Woan-Ruoh Lee<sup>4</sup>  
and Yong-Chien Ling<sup>1,2\*</sup>

<sup>1</sup>Department of Chemistry, National Tsing Hua University, Hsinchu 30013, Taiwan

<sup>2</sup>Biomedical Mass Imaging Research Center, Taipei Medical University, Taipei 11031, Taiwan

<sup>3</sup>Graduate Institute of Medical Science, Taipei Medical University, Taipei 11031, Taiwan

<sup>4</sup>Department of Dermatology, Taipei Medical University, Taipei 11031, Taiwan

\*ycling@mx.nthu.edu.tw

(Received : November 9, 2010; Accepted : January 15, 2011)

We prepared ZnO-containing nanomaterials of different-sized native ZnO and isotope-enriched  $^{68}\text{ZnO}$  nanoparticles (NPs) with well-characterized composition and applied them to HaCaT cells for *in vitro* cytotoxicity study. ToF-SIMS was applied to probe spatially-resolved intracellular changes. Elevated level of intracellular Zn correlated well with decreased  $^{39}\text{K}/^{40}\text{Ca}$  upon increased ZnO NPs exposure, indicating that the dissolving behavior of ZnO NPs played an important role in inducing cytotoxicity. Furthermore, the coherency of spatial distribution between elevated Zn and decreased  $^{39}\text{K}/^{40}\text{Ca}$  leads us to propose the presence of local cytotoxicity effect by ZnO NPs. Similar results were obtained irrespective of the use of native or isotope-enriched ZnO NPs, indicating the negligible contribution to cytotoxicity from intrinsic  $\text{Zn}^{2+}$ .

## 1. Introduction

The nano-scaled zinc oxide (ZnO) possessing many unique and advantageous properties is considered as the next most important nanomaterials (NMs) after carbon nanotubes [1]. The considerable rise of using NMs in industrial application has caused increased concerns of human exposure, rendering the safety evaluation of NMs being a priority issue [2-4]. Nanotoxicology, defined as “science of engineered nanodevices and nanostructures that deals with their effects in living organisms” [5], is expectedly becoming an important research field [6-8]. ZnO nanoparticles (NPs) of different size and shape have been reported to result in different extent of toxicological effects on cells and organisms. For example, acute oral toxicological impact on healthy adult mice study, however, revealed little difference in toxic effects between submicro- and nano-scaled ZnO particles (120 and 20 nm) [9]. Herein, we prepared ZnO NPs with well-characterized material properties, aiming to better understand the material characteristics effect on induced cytotoxicity.

The possibility of false positive results from spectroscopic interferences ( $^{40}\text{Ar}^{24}\text{Mg}$  on  $^{64}\text{Zn}$ ), non-spectroscopic interferences (matrix effects), and background interferences render trace element analysis in biological samples using mass spectrometry a challenging task [10]. Herein, we prepared  $^{68}\text{ZnO}$  NPs (98%  $^{68}\text{Zn}$  purity) as an isotopic tracer in dermal exposure experiment to discriminate signals from intrinsic Zn species. Intracellular and spatially-resolved chemical composition is critical for revealing the possible correlation between ZnO NPs and cytotoxicity effect. We used time of flight secondary ion mass spectrometry (ToF-SIMS) [11-13] as a rapid imaging tool for this purpose. To our knowledge, this is the first report using ToF-SIMS for *in vitro* cytotoxicity study of ZnO NPs on HaCaT cells.

## 2. Experimental

### 2.1 Reagents

Zinc acetate [ $\text{Zn}(\text{CH}_3\text{COO})_2 \cdot 2\text{H}_2\text{O}$ ] from Showa (Japan), oxalic acid ( $\text{H}_2\text{C}_2\text{O}_4 \cdot 2\text{H}_2\text{O}$ ) from Merck (Germany), and acetate acid ( $\text{CH}_3\text{COOH}$ ) of analytical grade from J.T. Baker (USA) were

used as received. Micro-sized  $^{68}\text{ZnO}$  powder from China Institute of Atomic Energy was used for preparing  $^{68}\text{ZnO}$  NPs. Fetal bovine serum (FBS) and Dulbecco's modified eagle medium (DMEM) from Invitrogen Corporation (USA), Penicillin-Streptomycin Amphotericin B solution (PSA) from Biological Industries (Israel), Trypsin-EDTA buffer (TE buffer), and phosphate buffered saline (PBS buffer) from Sigma-Aldrich (USA) were used as received. De-ionized (DI) water ( $> 18 \text{ M}\Omega\text{cm}^{-1}$ ) was obtained from a Milli-Q waters system (Millipore, USA).

## 2.2 Preparation of native ZnO and isotope-enriched $^{68}\text{ZnO}$ NPs

The ZnO NPs were prepared according to literature report [14]. The typical procedure involved slowly injecting 0.3 M  $\text{H}_2\text{C}_2\text{O}_4 \cdot 2\text{H}_2\text{O}$  solution into 0.2 M  $\text{Zn}(\text{CH}_3\text{COO})_2 \cdot 2\text{H}_2\text{O}$  solution with a syringe pump (KD Scientific, USA). The intermediate products ( $\text{ZnC}_2\text{O}_4$ ) obtained after 12 h continuous stirring were collected, rinsed with DI water, and freeze-dried to remove residuals. The ZnO NPs were obtained after 3 h calcination of the zinc oxalate at 400 °C. The  $^{68}\text{ZnO}$  NPs were prepared from micro-scaled  $^{68}\text{ZnO}$  powder. In brief, 3 mM  $\text{H}_2\text{C}_2\text{O}_4 \cdot 2\text{H}_2\text{O}$  solution was slowly injected into 50% acetate acid solution containing dissolved micro-scaled  $^{68}\text{ZnO}$ . Similar intermediate products ( $^{68}\text{ZnC}_2\text{O}_4$ ) were obtained and processed using procedure similar to ZnO NPs preparation to obtain  $^{68}\text{ZnO}$  NPs. The obtained NPs were used in all experimental works.

## 2.3 Characterization

The morphology of ZnO NPs was examined with a transmission electron microscope (TEM, JEOL 2010, Japan) operating at 200 kV by depositing sample onto the carbon-coated copper grids. The crystalline structure was determined using a powder X-ray diffraction (PXRD), which was performed on Shimadzu XD-5 diffractometer (Japan) operating with Cu K $\alpha$  radiation at 40 kV and  $\lambda = 0.1540 \text{ nm}$ . The mean hydrodynamic diameter of NPs was determined by a dynamic light scattering (DLS, Nano-ZS90, MALVERN, UK) instrument.

## 2.4 Cell culture and treatment with ZnO and $^{68}\text{ZnO}$ NPs

Human keratinocytes (HaCaT) cells, typically used *in vitro* toxicological experiments of skin damage or disease, were selected as the cellular model. The HaCaT cells were cultured in a medium (TE buffer, 10% FBS in DMEM, and

10% PSA, pH=6.5) and incubated at 37 °C under 5%  $\text{CO}_2$  humidified atmosphere. The HaCaT cells initially grew in  $1 \times 1 \text{ cm}^2$  silicon wafers (National Nano Device Laboratories, Taiwan) placed at the bottom of 24-well plate with a density of  $1.0 \times 10^5$  cells per well in 1.0 mL culture medium. The harvested cells were subsequently exposed to various dosage (10, 50, and 100  $\mu\text{g mL}^{-1}$ ) of ZnO (and  $^{68}\text{ZnO}$ ) NPs and cultured at 37 °C for 24 h, designated as experimental group. The control group was simultaneously prepared using similar procedures except using any ZnO (and  $^{68}\text{ZnO}$ ) NPs.

## 2.5 Cell pretreatment and ToF-SIMS analysis

The harvested HaCaT cells were subjected to 3-step molecular imprint [15] and freeze-dried pretreatment prior to ToF-SIMS analysis. In brief, the medium containing residual NPs on the sterilized Si wafers (designated as 1<sup>st</sup>) covered with harvested cells were washed off with PBS buffer. A sterilized Si wafer (designated as 2<sup>nd</sup>) was applied and pressed onto the cell-covered surface of 1<sup>st</sup> Si wafer in liquid nitrogen. After 10 min, the 2<sup>nd</sup> Si wafer fractured from the 1<sup>st</sup> Si wafer was pressed onto the Au top layer of a 3<sup>rd</sup> Si wafer in liquid nitrogen. The 3<sup>rd</sup> Si wafer fractured from the 2<sup>nd</sup> Si wafer was freeze-dried and subjected to ToF-SIMS analysis using a ToF-SIMS IV instrument (ION-TOF GmbH, Germany) operated at a mass resolution of  $\sim 6000$ . A primary ion gun consisting of 25 keV  $\text{Ga}^+$  ions with ion dose density ( $< 6.0 \times 10^8 \text{ ions cm}^{-2}$ ), beam radii of 2-10  $\mu\text{m}$ , and 1 pA pulse current was employed. The ion dose density is well below the co-called static limit,  $10^{13} \text{ ions cm}^{-2}$  [16]. Charge compensation with a pulsed flood low-energy electron gun was used. The ion images were reconstructed from the surface mass spectra scanned over a  $70 \mu\text{m} \times 70 \mu\text{m}$  field view.

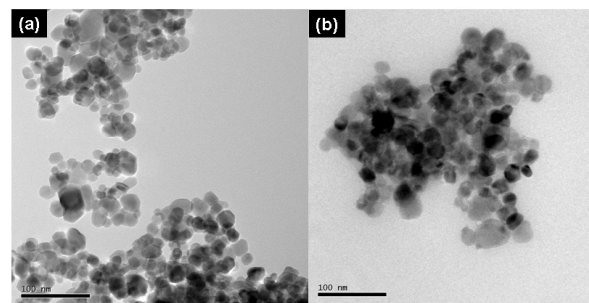


Fig. 1. The TEM images of (a) ZnO and (b)  $^{68}\text{ZnO}$  NPs, respectively.

### 3. Results and discussion

#### 3.1 Characterization of ZnO and $^{68}\text{ZnO}$ NPs

The particle size of the as-prepared ZnO and  $^{68}\text{ZnO}$  NPs measured by TEM (Fig. 1) is estimated ranging from 20-30 and 15-25 nm, respectively. Good agreement between the PXRD patterns (results not shown) of  $^{68}\text{ZnO}$  NPs and ZnO demonstrates successful preparation of  $^{68}\text{ZnO}$  NPs from micro-scaled  $^{68}\text{ZnO}$  powder.

#### 3.2 ToF-SIMS surface mass spectral analysis

The positive ion surface mass spectra of HaCaT cells from the control and experimental groups are shown in Fig 2. The  $^{39}\text{K}^+$ ,  $^{40}\text{Ca}^+$ , and  $^{64}\text{Zn}^+$  peak at  $m/z$  39, 40, and 64 displayed different variation trends, respectively. The peak intensity at  $m/z$  64 was presumably attributed to  $^{64}\text{Zn}$  dissolved from ZnO NPs considering the unfavorable ionization efficiency of ZnO under Ga ion bombardment. The absence of  $^{64}\text{Zn}^+$  peak in the mass spectrum of cells from control group (Fig 2a), implying that the amount of intrinsic  $^{64}\text{Zn}^+$  was below the detection limit of ToF-SIMS employed in this study. At  $10\ \mu\text{g mL}^{-1}$  exposure (Fig 2b), the  $^{64}\text{Zn}^+$  peak was still absent. However, the relative peak intensity of  $^{39}\text{K}^+$  to  $^{40}\text{Ca}^+$  became smaller. At higher exposure (50 and  $100\ \mu\text{g mL}^{-1}$ ), the  $^{64}\text{Zn}^+$  peak intensity continued elevating as shown in Fig 2c and 2d. A detailed inspection of the relative peak intensity of  $^{39}\text{K}/^{40}\text{Ca}$  indicated decreased  $^{39}\text{K}/^{40}\text{Ca}$  ratio with increased ZnO NPs exposure on HaCaT cells. In the control group (Fig 2a) and  $10\ \mu\text{g mL}^{-1}$  exposure experimental group (Fig 2b), the intensity of  $^{39}\text{K}^+$  peak was greater than  $^{40}\text{Ca}^+$ . In contrast, the  $^{40}\text{Ca}^+$  peak intensity became greater than  $^{39}\text{K}^+$  at higher exposure (50 and  $100\ \mu\text{g mL}^{-1}$ ) as shown in Fig 2c and 2d. The expression of cellular  $\text{K}^+$  and  $\text{Ca}^{2+}$  channels by stimulating/inhibiting receptors in cancer cells has been an intensive research subject. There are reports demonstrated that  $\text{K}^+$  channel activity was associated with  $\text{Ca}^{2+}$ -induced differentiation of human keratinocytes [17-18]. We presumed that the  $\text{Ca}^{2+}$  channel in cell membrane was activated once the HaCaT cells were exposed to high level of ZnO NPs and resulted in the expression of higher level of intracellular  $\text{Ca}^{2+}$ . As shown in Fig 2, the intracellular  $^{40}\text{Ca}^+$  peak intensity gradually elevated with increased ZnO NPs exposure. Accordingly, the  $\text{K}^+$  channel activated by elevated  $\text{Ca}^{2+}$  might progressively result in decreased intracellular  $^{39}\text{K}^+$  level as elucidated by ToF-SIMS results. The  $^{64}\text{Zn}^+$  dissolved from ZnO NPs might therefore play a critical role in inducing

cytotoxicity.

In order to assure  $^{64}\text{Zn}^+$  dissolved from ZnO NPs rather than the intrinsic  $^{64}\text{Zn}^+$  or other interfering species playing a critical role in inducing cytotoxicity, we performed similar exposure study using  $^{68}\text{ZnO}$  (98% purity) NPs as isotopic tracer. Fig 3 shows the positive ion surface mass spectra of HaCaT cells from control and experimental groups, respectively. Similar trends of increased  $^{68}\text{Zn}^+$  peak intensity correlating with decreased  $^{39}\text{K}/^{40}\text{Ca}$  ratio were observed, confirming that the dissolving behavior of ZnO NPs played an important role in inducing cytotoxicity. The results obtained were irrespective of using native ZnO NPs or  $^{68}\text{ZnO}$  NPs, indicating the negligible contribution to inducing cytotoxicity from intrinsic Zn species.

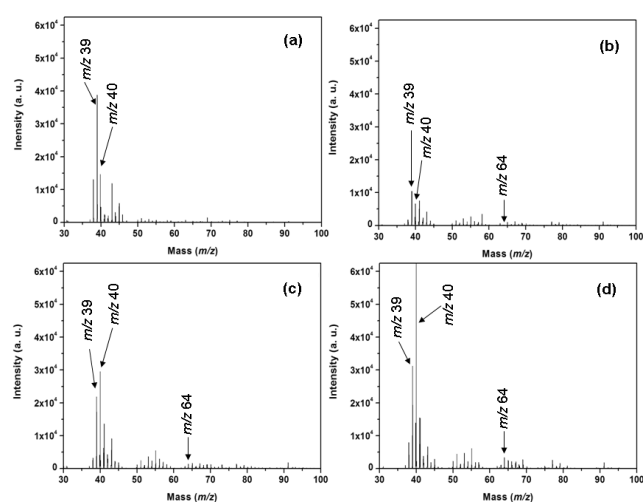


Fig. 2. The positive ion ToF-SIMS spectra of HaCaT cells from (a) control, and experimental group of (b) 10, (c) 50, and (d)  $100\ \mu\text{g mL}^{-1}$  ZnO NPs exposure.

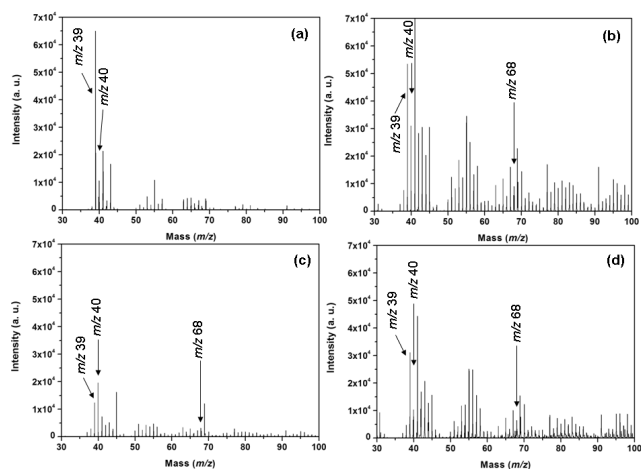


Fig. 3. The positive ion ToF-SIMS spectra of HaCaT cells from (a) control, and experimental group of (b) 10, (c) 50, and (d)  $100\ \mu\text{g mL}^{-1}$   $^{68}\text{ZnO}$  NPs exposure.

### 3.3 ToF-SIMS image analysis

The correlation between increased  $\text{Zn}^+$  peak intensity with decreased  $^{39}\text{K}/^{40}\text{Ca}$  ratio qualitatively mentioned above is quantitatively presented in Table 1. The ratio obtained representing an average value from a  $70\ \mu\text{m} \times 70\ \mu\text{m}$  field and gradually decreased from 5.43 to 5.18, 0.51, 0.14 and 6.61, to 2.20, 0.34, 0.13 for ZnO and  $^{68}\text{ZnO}$  NPs, respectively. At the highest  $100\ \mu\text{g mL}^{-1}$  exposure, similar ratio of 0.13~0.14 was obtained irrespective of the ZnO NPs used, implying that the HaCaT cells were extensively damaged. The heterogeneous distribution of ZnO NPs examined under scanning laser confocal microscopy (results not shown) in a separate study prompts us to investigate the possibility of local toxicity effect. Fig 4 shows the ToF-SIMS  $^{68}\text{Zn}^+$  image of HaCaT cells exposed to  $100\ \mu\text{g mL}^{-1}$   $^{68}\text{ZnO}$  NPs. The  $^{39}\text{K}/^{40}\text{Ca}$  ratio spatially fluctuated. For example, the ratio is 0.1, 1.1, and 0.8 in  $^{68}\text{Zn}$ -enriched (Fig 4a) and  $^{68}\text{Zn}$ -poor (Fig 4b and 4c) area, respectively. This coherency of spatial distribution between elevated  $\text{Zn}^+$  and decreased  $^{39}\text{K}/^{40}\text{Ca}$  lead us to propose the presence of local cytotoxicity effect by Zn-containing species from ZnO NPs. However, the exact location of the hot spot is unclear based on current data. Future work is warranted toward this end.

Table 1. The correlation between ZnO (or  $^{68}\text{ZnO}$ ) NPs dosage and  $^{39}\text{K}/^{40}\text{Ca}$  ratio.

Dosage ( $\mu\text{g mL}^{-1}$ )	$^{39}\text{K}/^{40}\text{Ca}$	
	ZnO	$^{68}\text{ZnO}$
0	5.43	6.61
10	5.18	2.20
50	0.51	0.34
100	0.14	0.13

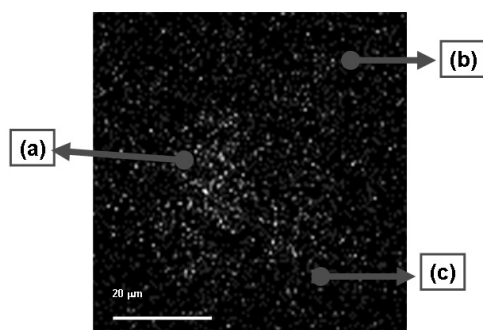


Fig. 4. The ToF-SIMS  $^{68}\text{Zn}^+$  image of HaCaT cells exposed to  $100\ \mu\text{g mL}^{-1}$   $^{68}\text{ZnO}$  NPs. (a)  $^{68}\text{Zn}$ -enriched area; (b) and (c)  $^{68}\text{Zn}$ -poor area.

### 4. Conclusions

This study demonstrated that ToF-SIMS successfully revealed the intracellular changes of specific ion species induced by ZnO NPs on HaCaT cells. The elevated level of dissolved Zn ions from ZnO NPs correlated with decreased  $^{39}\text{K}/^{40}\text{Ca}$  ratio was revealed from ToF-SIMS surface mass spectral analysis, indicating that the dissolving behavior of ZnO NPs played an important role in inducing cytotoxicity. The coherency of spatial distribution between elevated  $\text{Zn}^+$  and decreased  $^{39}\text{K}/^{40}\text{Ca}$  revealed by ToF-SIMS image analysis indicates the presence of local cytotoxicity effect by ZnO NPs. The isotope-enriched  $^{68}\text{ZnO}$  NPs possessing material characteristics similar to native ZnO NPs is a potential tracer in ZnO NPs research for discriminating possible effect from intrinsic Zn species. Label-free ToF-SIMS might open up new avenues and become a paradigm tool for nanotoxicology research.

### Acknowledgement

We gratefully acknowledge the financial support from the National Science Council, Taiwan (NSC 98-2113-M-007-016-MY3), National Tsing Hua University (98N2570E1), and Taipei Medical University.

### References

- [1] Z. L. Wang, X. Y. Kong, Y. Ding, P. X. Gao, W. L. Hughes, R. S. Yang, and Y. Zhang, *Adv. Funct. Mater.*, **14**, 943 (2004).
- [2] K. Ghule, A. V. Ghule, B. J. Chen, and Y. C. Ling, *Green Chem.*, **8**, 1034 (2006).
- [3] S. George, S. Pokhrel, T. Xia, B. Gilbert, Z. X. Ji, M. Schowalter, A. Rosenauer, R. Damoiseaux, K. A. Bradley, L. Madler, and A. E. Nel, *ACS Nano*, **4**, 15 (2010).
- [4] J. X. Wang, C. Y. Chen, Y. Liu, F. Jiao, W. Li, F. Lao, Y. F. Li, B. Li, C. C. Ge, G. Q. Zhou, Y. X. Gao, Y. L. Zhao, and Z. F. Chai, *Toxicol Lett*, **183**, 72 (2008).
- [5] G. Oberdorster, E. Oberdorster, and J. Oberdorster, *Environ. Health Persp.*, **113**, 823 (2005).
- [6] A. D. Maynard, R. J. Aitken, T. Butz, V. Colvin, K. Donaldson, G. Oberdorster, M. A. Philbert, J. Ryan, A. Seaton, V. Stone, S. S. Tinkle, L. Tran, N. J. Walker, and D. B. Warheit, *Nature*, **444**, 267 (2006).
- [7] A. Nel, T. Xia, L. Madler, and N. Li, *Science*, **311**, 622 (2006).
- [8] V. H. Grassian, P. T. O'Shaughnessy, A. Adamcakova-Dodd, J. M. Pettibone, and P. S.

Thorne, *Environ. Health Persp.*, **115**, 397 (2007).

[9] B. Wang, W. Y. Feng, M. Wang, T. C. Wang, Y. Q. Gu, M. T. Zhu, H. Ouyang, J. W. Shi, F. Zhang, Y. L. Zhao, Z. F. Chai, H. F. Wang, and J. Wang, *J. Nanopart. Res.*, **10**, 263 (2008).

[10] J. H. Wang, and E. H. Hansen, *J. Anal. Atom. Spectrom.*, **16**, 1349 (2001).

[11] S. Vaidyanathan, J. S. Fietcher, R. Goodacre, N. P. Lockyer, J. Micklefield, and J. C. Vickerman, *Anal. Chem.*, **80**, 1942 (2008).

[12] S. L. Lei, Y. S. Yin, P. L. Lee, and Y. C. Ling, *Surface and Interface Analysis*, **in press**, (2010).

[13] S. Aoyagi, A. Takesawa, A. C. Yamashita, and M. Kudo, *Appl. Surf. Sci.*, **252**, 6697 (2006).

[14] K. G. Kanade, B. B. Kale, R. C. Aiyer, and B. K. Das, *Mater. Res. Bull.*, **41**, 590 (2006).

[15] P. Sjoval, J. Lausmaa, H. Nygren, L. Carlsson, and P. Malmberg, *Anal. Chem.*, **75**, 3429 (2003).

[16] J. C. Vickerman, in *ToF-SIMS : surface analysis by mass spectrometry*, by J. C. Vickerman and D. Briggs, pp. 285-308, IM Publications and SurfaceSpectra Limited, Chichester (2001).

[17] A. Arcangeli, and A. Becchetti, *Trends Cell Biol.*, **16**, 631 (2006).

[18] H. Koegel, and C. Alzheimer, *Faseb J*, **15**, 145 (2001).